

We are IntechOpen, the world's leading publisher of Open Access books Built by scientists, for scientists

6,900

Open access books available

185,000

International authors and editors

200M

Downloads

Our authors are among the

154

Countries delivered to

TOP 1%

most cited scientists

12.2%

Contributors from top 500 universities



WEB OF SCIENCE™

Selection of our books indexed in the Book Citation Index
in Web of Science™ Core Collection (BKCI)

Interested in publishing with us?
Contact book.department@intechopen.com

Numbers displayed above are based on latest data collected.
For more information visit www.intechopen.com



Synthesis and Study of Structural and Dielectric Properties of Dy-Ho Doped Mn-Zn Ferrite Nanoparticles

*Krishtappa Manjunatha,
Veerabhadrapa Jagadeesha Angadi,
Brian Jeevan Fernandes and
Keralapura Parthasarathy Ramesh*

Abstract

The Dy-Ho doped Mn-Zn Ferrite nanoparticles have been synthesized by solution combustion method using mixture of fuels as glucose and urea. The synthesized samples of structural properties were characterized through XRD (X-ray diffraction) and dielectric properties were studied through impedance analyzer. The XRD patterns of all samples confirms the spinel cubic structure having space group $Fd\bar{3}m$. Further all synthesized samples reveal the single-phase formation without any secondary phase. The lattice parameters and hopping lengths were increases with increase of Dy-Ho concentration. SEM micrographs shows the porous nature for all samples. The crystallite size increases with increase of Dy-Ho concentration. The Dielectric properties of all the samples were explained by using Koop's phenomenological theory. The real part of dielectric constant, imaginary part of dielectric constant and dielectric loss tangent were decreases with increase of frequency. The AC conductivity increases with increase of frequency. The real part of impedance spectra decreases with increase of frequency for all samples. The Cole-Cole plots shows the one semicircle for all samples. The high ac conductivity and low dielectric loss observed for all samples at high frequency region and this samples are reasonable for power transformer applications at high frequencies.

Keywords: Mn-Zn Ferrite nanoparticles, solution combustion method, Koop's phenomenological theory, Cole-Cole plots

1. Introduction

Nano-ferrites, which are currently being studied, have piqued curiosity on account of their remarkable electrical properties. Due to their extraordinary physical and chemical properties, spinel ferrites nanoparticles have become a significant field of research in nanotechnology, nanoscience, and nanoelectronics [1–6]. A kind of high resistance spinel ferrite with a conventional AFe_2O_4 formula, where A alludes to divalent (+2) metal ions. In deciding their significant applications, dielectric and

electrical examinations of spinel ferrites assume a vital role. Doping has a considerable impact on the semiconductive property of spinel ferrites. The high electrical resistance of soft ferrites, which prevents undesirable eddy current losses in AC fields, is the most important asset they create for being qualified for high-frequency applications. Spinel ferrites might be utilized in a MCS (microwave communication system) [7], magnetic transmitter feeder [8], pulsed current monitor [9] and gas sensor [10]. Spinel ferrites, on the other hand, have excellent chemical stability and biocompatibility under physiological conditions [11]. Impedance spectroscopy was used to explore the electrical characteristics of spinel ferrites. Electrical similar circuits with inductors, capacitors and resistors are commonly utilized models for complex impedance. A comprehensive impedance examination can provide the necessary information of a material's dielectric characteristics. This research enables for the separation of distinct total impedance contributions arising from bulk conductivity and interfacial phenomena, such as grain boundary, grain, and other electrode interface results.

Mn-Zn ferrites are relied upon to be mixed ferrites with $\text{Fe}^{2+}/\text{Fe}^{3+}$ ions affecting dielectric characteristics at both A-site and B-site. As a result, Mn-Zn ferrites offer a wide range of electrical properties that can be applied to a wide range of technological applications, including telecommunications [12]. Few researchers are researching the effect of rare earth such as Sm, Gd, Eu, and Ce among others, on the varied properties of Mn-Zn ferrite, according to a thorough literature assessment [13, 14]. The dielectric properties of $\text{Zn}_{0.2}\text{Ni}_{0.8-x}\text{Cu}_x\text{Fe}_2\text{O}_4$ ($x = 0$ to 0.6) can be enhanced by replacing Ni^{2+} with Cu^{2+} , according to Houshair et al. Rao et al. [15] examined on the cation distribution of Ni-Zn-Mn ferrite NPs. Bharamagoudar et al. [16] reported that the $\text{Mn}_{1-x}\text{Zn}_x\text{Fe}_2\text{O}_4$ (where, $x = 0, 0.25, 0.5, 0.75, 1$) were prepared by solution combustion method and the dielectric constant decrements with enhancing of Zn content. In addition, Qian et al. [17] found that introducing Nd into Ni-Zn ferrite increased the dielectric properties. Impedance spectroscopy, in particular, has been carried out in various research. Rare earth (RE) metal ions (Dy&Ho) with larger ionic radii can cause crystal structure distortions [18]. As a result, replacing trivalent iron with RE metal ions at the Fe site improves dielectric and structural properties in Mn-Zn ferrites. There have been several studies on the integration of RE ions into Mn-Zn ferrites.

The main goal of this work is therefore to understand the dielectric constant, dielectric loss tangent, ac conductivity, cole-cole plot and impedance spectroscopy of Dy-Ho doped Mn-Zn ferrite. As indicated by the investigation accomplished, replacing of Fe^{3+} ions with a larger Dy^{3+} - Ho^{3+} ions results in a significant rise in dielectric and ac conductivity. In our current paper, we investigated the structure, dielectric properties of the current systems.

2. Synthesis method and characterizations

Stoichiometric quantity of metal nitrates such as manganese nitrate, zinc nitrate, ferrous nitrate, dysprosium nitrate, holmium nitrate and reducing agents as stoichiometry quantities of fuels glucose and urea were mixed in 30 ml distilled water, and the combined solution was taken in a borosil glass beaker. Then combined solution was continuously stirred for 60 min to achieve a homogeneous solution. At 450°C , this homogeneous solution was kept in a box style muffle furnace that had been preheated. The solution boils, froths, and then burns with a smoldering flame at first. The combustion process will be completed within 20 minutes. The flow chart of solution combustion method as shown in **Figure 1**.

The XRD was characterized by utilizing CuK_α radiation ($\lambda = 1.5406 \text{ \AA}$) and the 2 θ diffractogram was run from 20° to 80° with a stage size of 0.02 . We can deduce crystalline phase and structure from XRD patterns. The surface morphology of the all

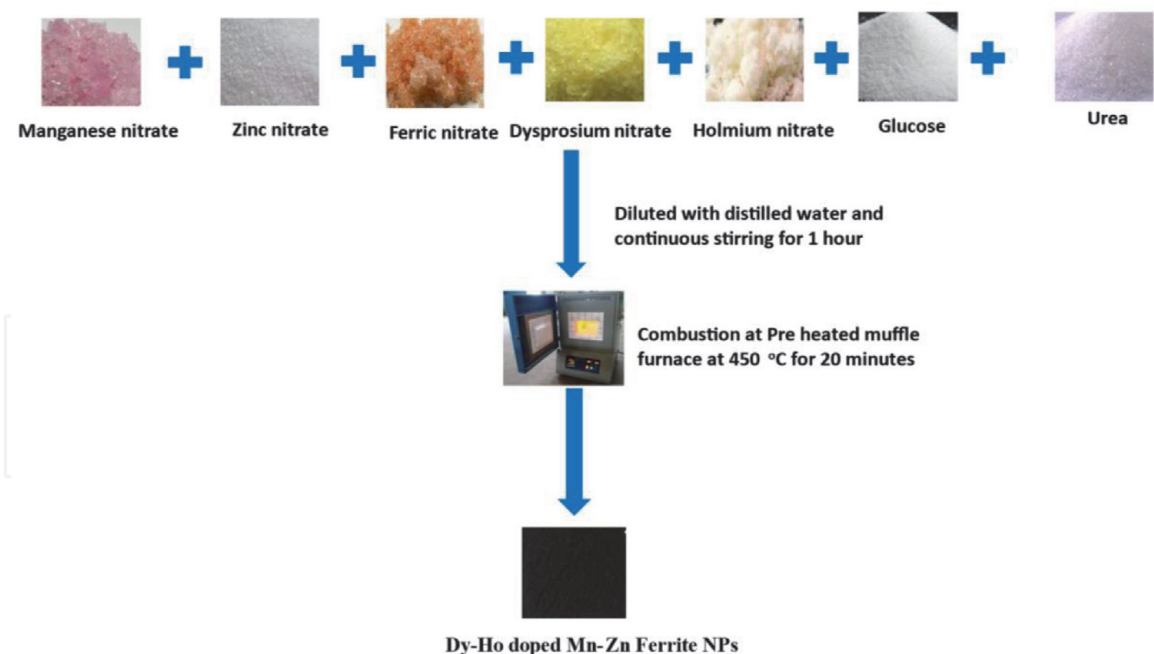


Figure 1.
Flow chart of solution combustion method for Dy-Ho doped M-Zn Ferrite NPs.

samples were analyzed by SEM images and the images were carried out by using JEOL (model JSM-840). For dielectric studies, the pellet of the sample was prepared using hydraulic press. The silver was pasted on it to get the electrical contact and heated in an oven for 2 hours at 55°C. The impedance spectroscopy measurement was performed in the frequency range up to 10 MHz using an Novocontrol Alfa A impedance analyzer.

3. Results

3.1 Structural analysis

The **Figure 2** depicts the XRD pattern of $\text{Mn}_{0.5}\text{Zn}_{0.5}\text{Dy}_x\text{Ho}_y\text{Fe}_{2-x-y}\text{O}_4$ ($x = y = 0.005, 0.010, 0.015, 0.020, 0.025$ and 0.030) NPs. The single-phase cubic structure was verified for all samples, and the pattern matched data card ICDD#10–0319 perfectly. The miller indices (hkl) suggested a spinel cubic structure without appearance of secondary phases. The lattice constant (a) values of were estimated by using the following relation [19].

$$a = \frac{\lambda \sqrt{h^2 + k^2 + l^2}}{2 \sin \theta} \quad (1)$$

For $x = y = 0.005$ to 0.03 concentration, the values of ‘a’ were found 8.3964 to 8.4245 Å, respectively. Eq. (1) was utilized to estimate the crystallite size of $\text{Mn}_{0.5}\text{Zn}_{0.5}\text{Dy}_x\text{Ho}_y\text{Fe}_{2-x-y}\text{O}_4$ ($x = y = 0.005, 0.010, 0.015, 0.020, 0.025$ and 0.030) NPs using the Debye Scherrer Equation [20, 21];

$$D = \frac{k \lambda}{\beta \cos \theta} \quad (2)$$

The “λ” denotes the X-ray wavelength, the “β” denotes the FWHM value, k is the Scherrer constant and θ denotes the diffraction angle. The crystallite sizes measured were 11.88 to 6.44 nm for $x = 0.005$ to 0.03 , respectively. Large ionic radius of rare-

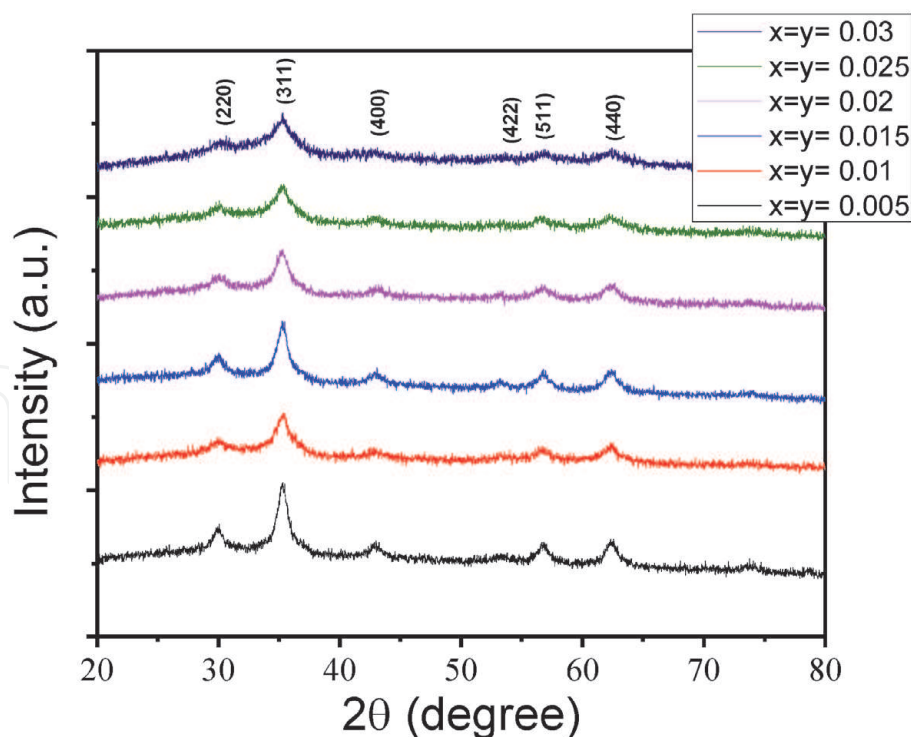


Figure 2.

The XRD patterns of $Mn_{0.5}Zn_{0.5}Dy_xHo_yFe_{2-x-y}O_4$ ($x = y = 0.005, 0.010, 0.015, 0.020, 0.025$ and 0.030) NPs.

earth ions increases the lattice parameter value while decreasing the average crystallite size, which is a popular trend [22]. However, in some cases, such as in our investigation, the researcher found different actions. The introduction of the Dy^{3+} - Ho^{3+} ions cause increases in the lattice parameter in our analysis. As the large ionic radius of Dy^{3+} (0.912 Å) and Ho^{3+} (0.901 Å) ions replaces the small ionic radius of Fe^{3+} (0.645 Å) ion at the B-site position, the lattice structure becomes asymmetric [23]. The hopping length at tetrahedral and octahedral sites was estimated by using following equations

$$L_A = \frac{\sqrt{3}a}{4} \text{ and } L_B = \frac{\sqrt{2}a}{4} \quad (3)$$

and observed the increase of hopping lengths with the increase of Ho^{3+} content as the lattice parameter increased gradually [24].

3.2 SEM analysis

SEM micrographs of $Mn_{0.5}Zn_{0.5}Dy_xHo_yFe_{2-x-y}O_4$ ($x = y = 0.005, 0.010, 0.015, 0.020, 0.025$ and 0.030) nanoparticles are shown in **Figure 3**. The existence of surface morphology with pores, holes, and on their surfaces can be seen in the figures. The development of the fuels during the combustion process resulted in the formation of the dry frothy powder. We are unable to measure grain size due to the porous nature of the samples. The micrographs show that the particles are agglomerated, showing that the magnetic nanoparticles in powder form have a strong connection [25].

3.3 Dielectric studies

3.3.1 Real part of dielectric constant

The variation of real part of dielectric constant (ϵ') with applied frequency as shown in **Figure 4**. The ϵ' reduces as the frequency increases, stays constant at higher frequencies, and declines as the Dy^{3+} and Ho^{3+} content increases. This

behavior could be explained by using Koop's theory. In the lower frequency zone, the electrons exchange between ions follows the applied electric field and is responsible for high value of ϵ' [26]. Due of high conducting grains, the ϵ' is

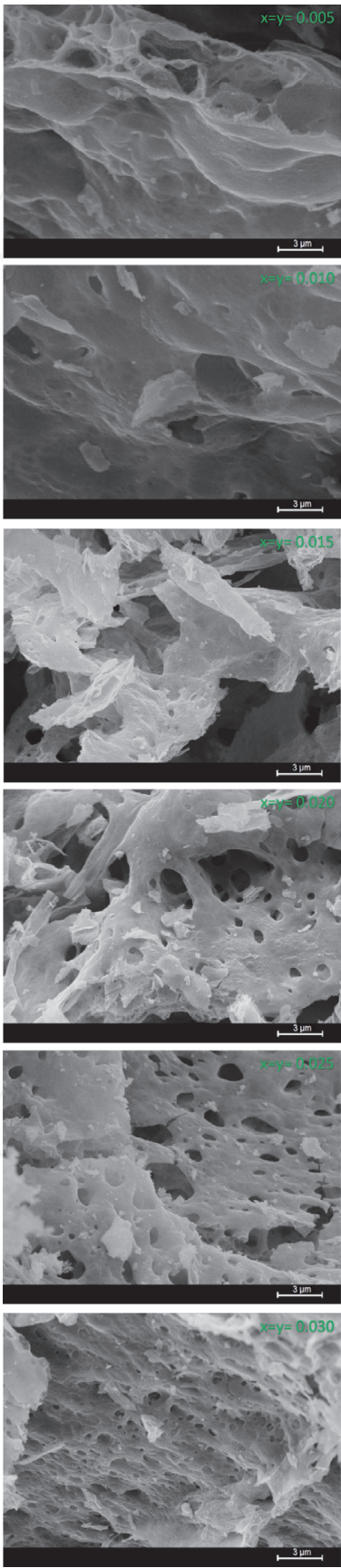


Figure 3.
SEM micrographs of $Mn_{0.5}Zn_{0.5}Dy_xHo_yFe_{2-x-y}O_4$ ($x = y = 0.005, 0.010, 0.015, 0.020, 0.025$ and 0.030) nanoparticles.

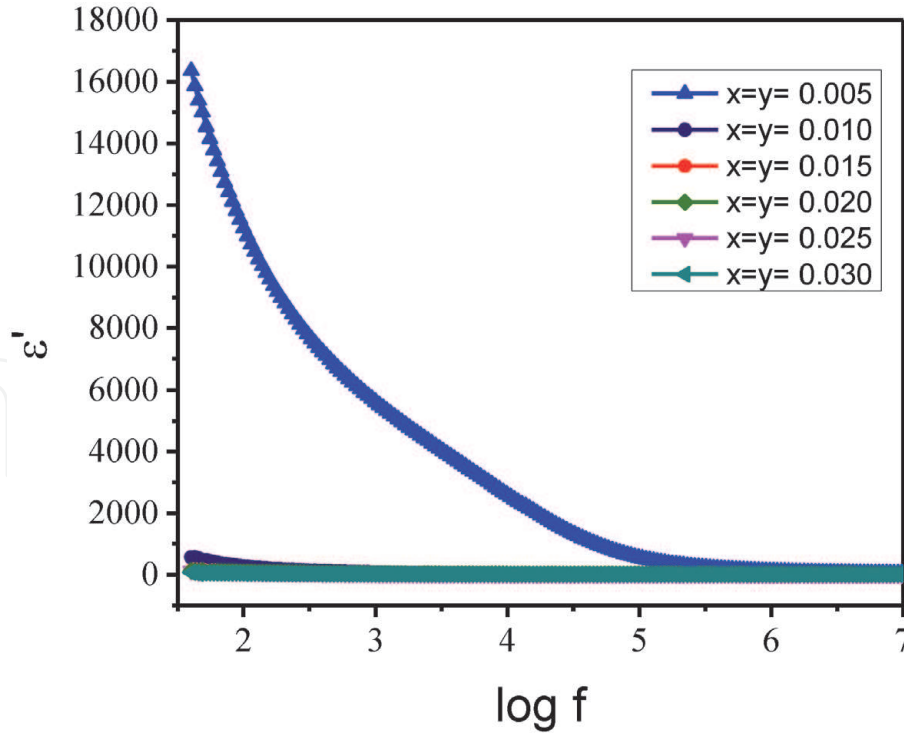


Figure 4. The variation of real part of dielectric constant (ϵ') with applied frequency of $Mn_{0.5}Zn_{0.5}Dy_xHo_yFe_{2-x-y}O_4$ ($x = y = 0.005, 0.010, 0.015, 0.020, 0.025$ and 0.030) NPs.

frequency independent at higher frequency region. The ionic and orientation polarizations weaken and eventually disappear as frequency rises, resulting in a drop in dielectric constant at higher frequency region [27]. Polarization is caused by electron exchange between Fe^{3+} and Fe^{2+} ions on the octahedral site in the ferrite lattice at lower frequencies.

3.3.2 Imaginary part of dielectric constant

The variation of real part of dielectric constant (ϵ'') with applied frequency as shown in **Figure 5**.

The concept of polarization and the hopping process can be used to understand the dielectric behavior of ferrite materials [28]. The following is the explanation for the observed dielectric loss in the ferrite samples: at lower frequency region the electron exchange between Fe^{2+} and Fe^{3+} is predominant and it follows the applied electric field. As the increase of frequency, the electron exchange between Fe^{2+} and Fe^{3+} ions does not follow the applied electric field.

3.3.3 Dielectric loss tangent

The variation of dielectric loss tangent ($\tan \delta$) with applied frequency as shown in **Figure 6**. Dielectric loss tangent in the ferrites is due to the lag of polarization with respect to the applied field [29, 30]. Ferrites with high $\tan \delta$ are suitable candidates for the manufacturing of high frequency heating systems. $\tan \delta$ decreases with the applied frequency for each sample. This can be ascribed based on Koop's phenomenological model [31, 32]. At low frequencies region non conducting grain boundary gives maximum contribution for polarization. At lower frequency grain boundary contribution dominates results high resistivity and high value of dielectric loss tangent. Large quantity of energy is required for electron exchange

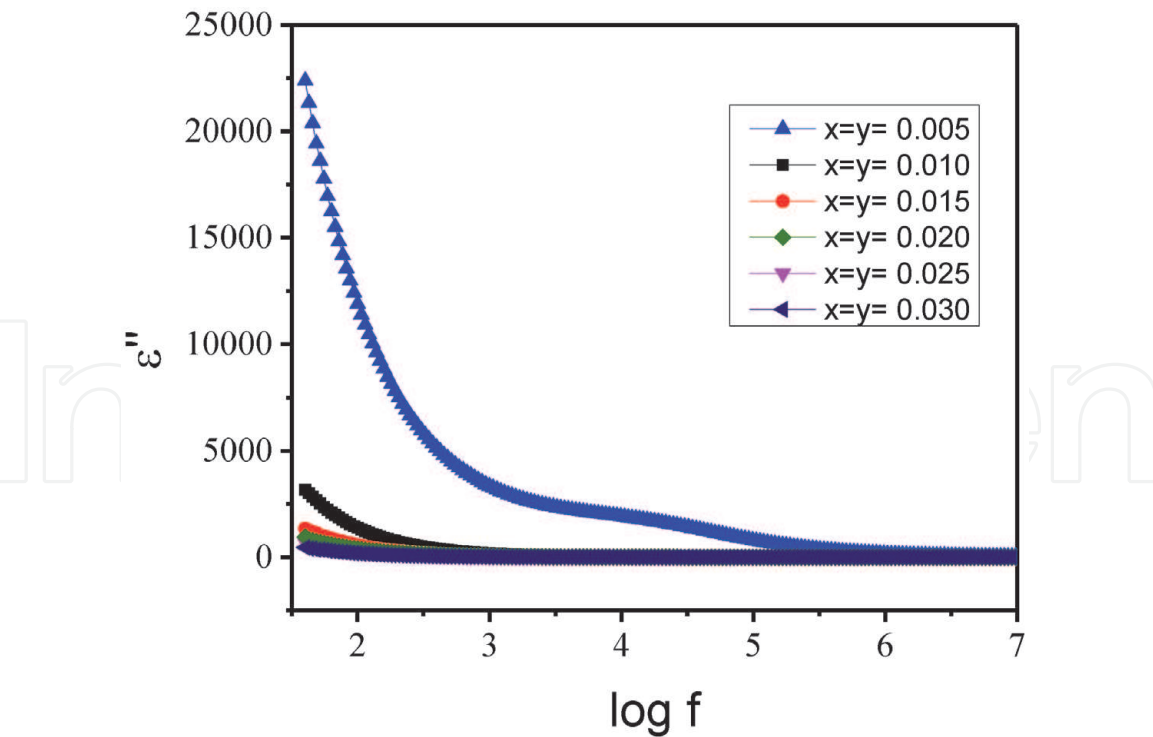


Figure 5.
 The variation of imaginary part of dielectric constant with applied frequency of $Mn_{0.5}Zn_{0.5}Dy_xHo_yFe_{2-x-y}O_4$ ($x = y = 0.005, 0.010, 0.015, 0.020, 0.025$ and 0.030) NPs.

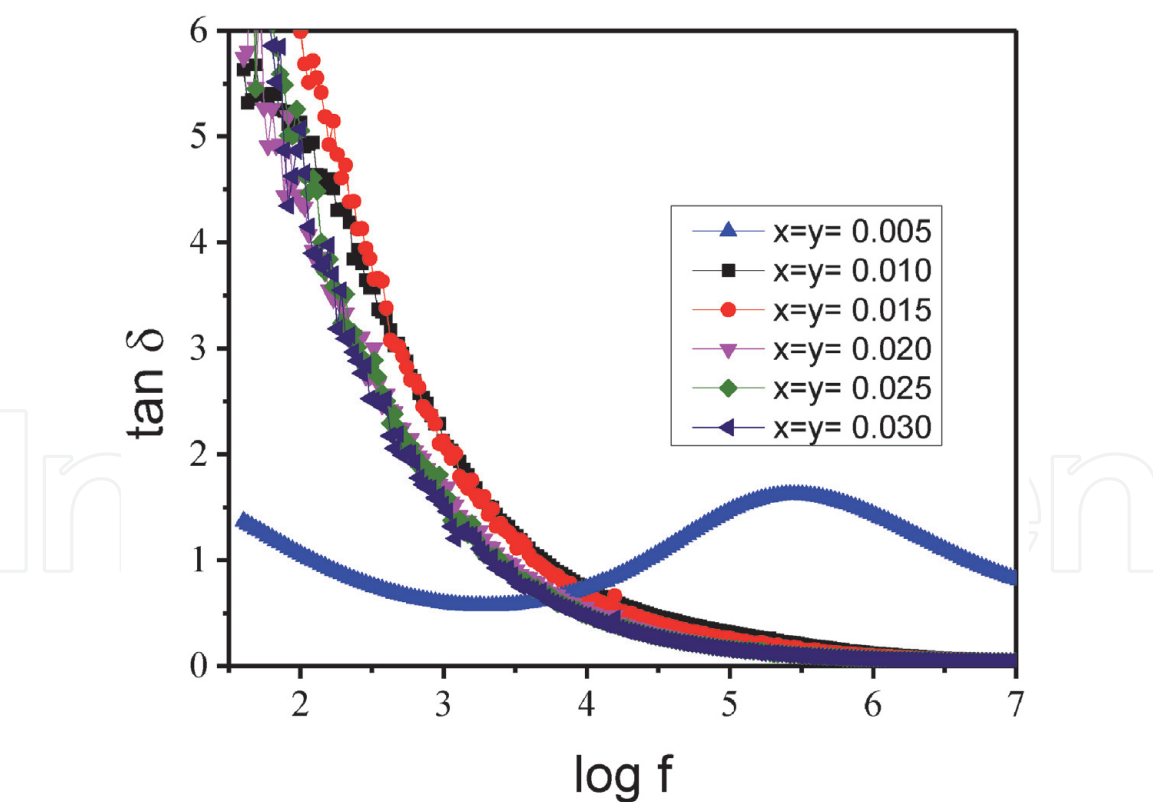


Figure 6.
 The variation of dielectric loss tangent with applied frequency of $Mn_{0.5}Zn_{0.5}Dy_xHo_yFe_{2-x-y}O_4$ ($x = y = 0.005, 0.010, 0.015, 0.020, 0.025$ and 0.030) NPs.

between Fe^{3+} ions and Fe^{2+} ions at low frequency ensuing high value of loss tangent. At higher frequencies, small quantity of energy is enough for exchange of electron between Fe^{2+} and Fe^{3+} gives low resistivity and low value of loss tangent [33, 34]. At $x = y = 0.005$ concentration sample shows hump at mid of the frequencies, which

was happened due to exchange of electron between ions frequency is matched with the applied frequency [35].

3.3.4 AC conductivity

The variation of AC conductivity (σ_{ac}) with applied frequency as shown in **Figure 7**. The frequency enhances with diminishing in σ_{ac} which can be explained due to hopping model. At lower frequency side independent of conductivity, so the σ_{ac} is small at lower frequency side. The Ho^{3+} - Dy^{3+} ions substitution on Fe^{3+} ions of B- site, here the electron exchange between ions and there is no electrons exchange between A site-B site. The electron exchange between A site-B site is most significant contrast with A site- A site and B site-B Site of spinel ferrite sample. The conduction mechanism enhances with enhancing the polarization there by enhancing the σ_{ac} [36].

3.3.5 Real part of impedance (Z') and imaginary part of impedance (Z'')

The variation of real part of impedance (Z') with applied frequency as shown in **Figure 8**. The spectra unmistakably shows that the Z' is diminishes with enhancing the frequency. Furthermore, because to the charge space polarization of the spinel ferrite sample [37], it remains constant at high frequency region. The imaginary part of impedance (Z'') varies with applied frequency, as shown in **Figure 9**. This spectrum (Z'' V/s log f) also named as loss spectrum. The frequency grows as Z'' decreases, and it reaches its maximum value at a certain frequency. The frequency then increases as Z'' decreases. Furthermore, the highest peak value rises as the concentrations of dysprosium and holmium rise. It results in the presence of relaxation time in the samples, which occurs as a result of space charge relaxation, which occurs when the sample is made up of grain borders and grain [38]. Furthermore, as the frequency shifts from low to high, the conduction mechanism shifts as well.

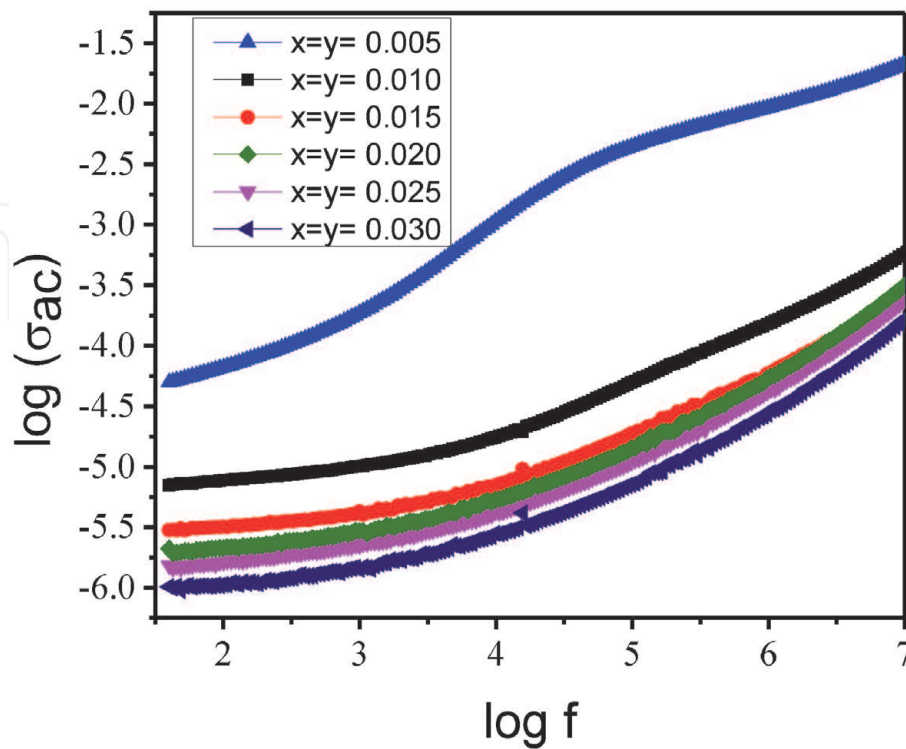


Figure 7.
The variation of AC conductivity with applied frequency of $\text{Mn}_{0.5}\text{Zn}_{0.5}\text{Dy}_x\text{Ho}_y\text{Fe}_{2-x-y}\text{O}_4$ ($x = y = 0.005, 0.010, 0.015, 0.020, 0.025$ and 0.030) NPs.

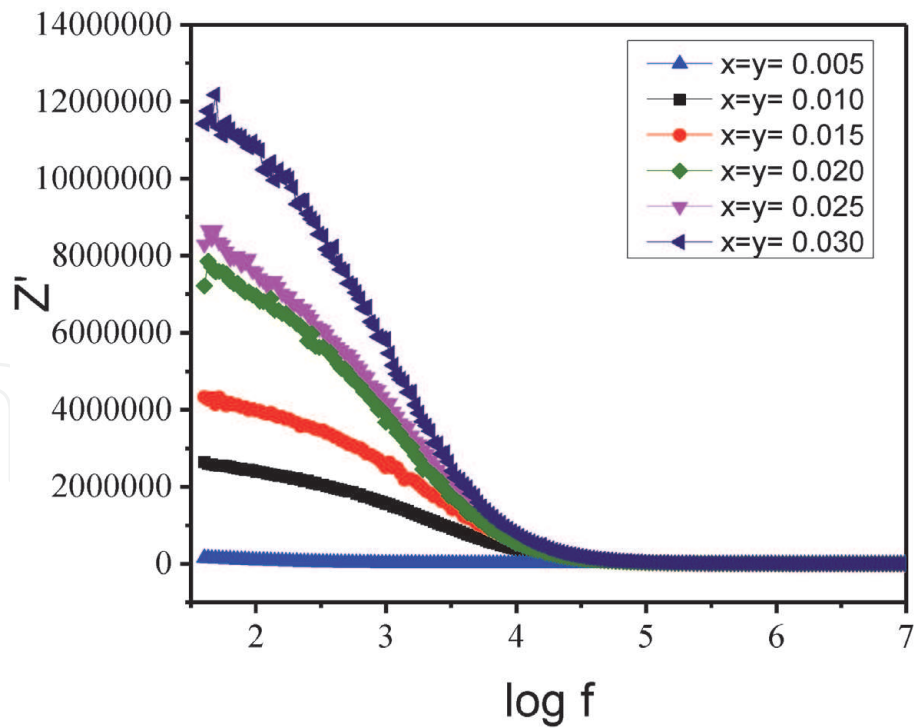


Figure 8.
 The variation of real part of impedance (Z') with applied frequency of $Mn_{0.5}Zn_{0.5}Dy_xHo_yFe_{2-x-y}O_4$ ($x = y = 0.005, 0.010, 0.015, 0.020, 0.025$ and 0.030) NPs.

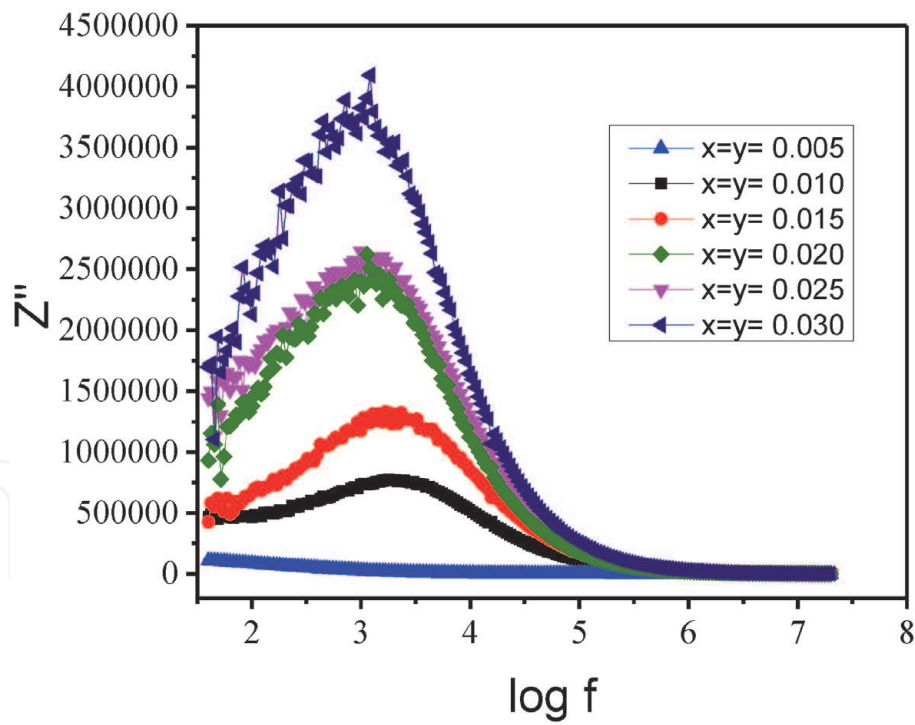


Figure 9.
 The variation of imaginary part of impedance (Z'') with applied frequency of $Mn_{0.5}Zn_{0.5}Dy_xHo_yFe_{2-x-y}O_4$ ($x = y = 0.005, 0.010, 0.015, 0.020, 0.025$ and 0.030) NPs.

3.3.6 Cole-Cole plot

The Cole-Cole plots (Z'' along y-axis and Z' along x-axis) as shown in **Figure 10**. shows the and this plot is called Cole-Cole plots. The occurrence of a non-Debye kind of relaxation phenomenon in the Dy-Ho doped Mn-Zn ferrite NPs is confirmed by the Cole-Cole plots complex impedance spectra of the semicircle spectra.

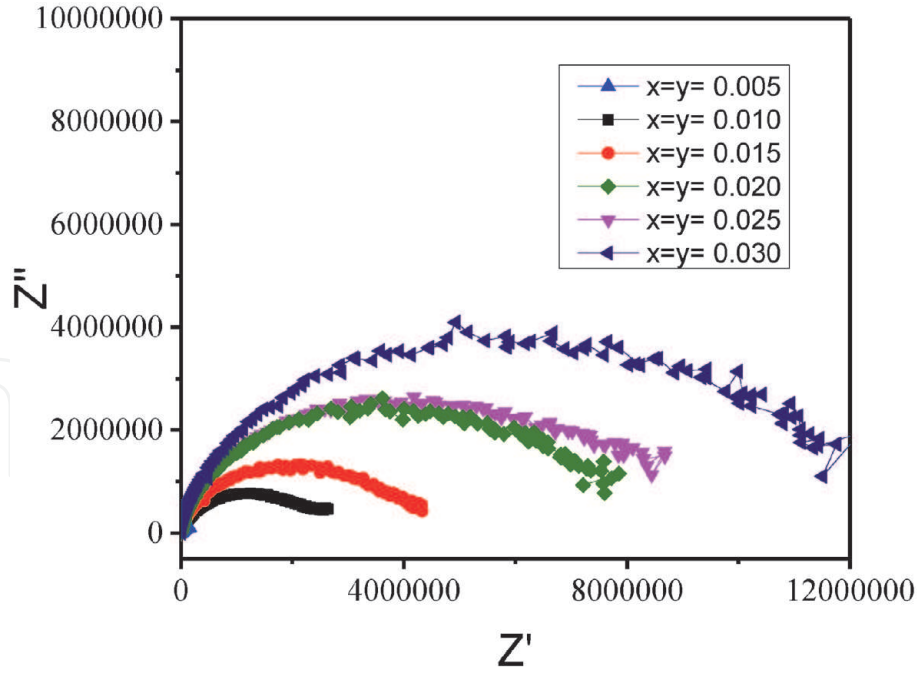


Figure 10.

Cole-Cole plots of $Mn_{0.5}Zn_{0.5}Dy_xHo_yFe_{2-x-y}O_4$ ($x = y = 0.005, 0.010, 0.015, 0.020, 0.025$ and 0.030) NPs.

Further, the maximum peak increases with increasing the Dy-Ho concentration. For the analogous circuit model, three series sets of capacitance and resistance are created in parallel. The complex impedance formula of an equivalent circuit is shown in Eq. (4) [39, 40].

$$Z = Z_0 + iZ'' = (1/R_b + i\omega C_b)^{-1} + (1/R_{gb} + i\omega C_{gb})^{-1} + (1/R_{el} + i\omega C_{el})^{-1} \quad (4)$$

Where R_b is the resistance of the material and C_b is the capacitance of the material, R_{el} and C_{el} is the contact impedance between material in the electrode. The capacitance and resistance assigned by C_{gb} and R_{gb} , respectively and brought about by the combination of grain boundary.

4. Conclusions

The synthesis of $Mn_{0.5}Zn_{0.5}Dy_xHo_yFe_{2-x-y}O_4$ ($x = y = 0.005, 0.010, 0.015, 0.020, 0.025$ and 0.030) NPs by solution combustion technique. The lattice parameters increases with increase of Dy-Ho content due to ionic radius of Dy^{3+} (0.912 Å) and Ho^{3+} (0.901 Å) ions greater than of Fe^{3+} (0.645 Å) ions. SEM micrographs shows the porous nature for all samples. The development of the fuels during the combustion process resulted in the formation of the dry frothy powder. The Dielectric properties of all the samples were explained by using Koop's phenomenological theory. The ϵ' , ϵ'' and $\tan\delta$ were decreases with increase of frequency. Dielectric loss tangent in the ferrites is due to the lag of polarization with respect to the applied field. The AC conductivity rises as the frequency rises. For all samples, the real part of the impedance spectra diminishes as the frequency increases. Noticed that the maximum peak value increases with increase of dysprosium and holmium content in the imaginary part of impedance spectra. It gives a presence of relaxation time in the samples and it happened due to the space charge relaxation that overwhelms when the sample is composed of grain boundaries and grain. The appearance of a non-Debye type of relaxation phenomenon is linked to the presence of a single semicircle in the Cole-Cole plots for all samples. The high ac conductivity and low

dielectric loss noticed for all samples at high frequency region are reasonable for power transformer applications at high frequencies.

Acknowledgements

Brian Jeevan Fernandes thanks University Grant Commission, Govt of India for the Dr. D.S. Kothari Post Doctoral Fellowship.

Author details

Krishtappa Manjunatha¹, Veerabhadrapa Jagadeesha Angadi^{2*},
Brian Jeevan Fernandes³ and Keralapura Parthasarathy Ramesh³


¹ Department of Physics, School of Engineering, Presidency University, Bangalore, India

² Department of Physics, P.C. Jabin Science College, Hubballi, India

³ Department of Physics, Indian Institution of Science (IISc), Bangalore, India

*Address all correspondence to: jagadeeshbub@gmail.com

IntechOpen

© 2021 The Author(s). Licensee IntechOpen. This chapter is distributed under the terms of the Creative Commons Attribution License (<http://creativecommons.org/licenses/by/3.0>), which permits unrestricted use, distribution, and reproduction in any medium, provided the original work is properly cited. 

References

- [1] S. Amiri, H. Shokrollahi, The role of cobalt ferrite magnetic nanoparticles in medical science, *Mater. Sci. Eng.: C*, 33 (2013) 1–8.
- [2] X. Meng, H. Li, J. Chen, L. Mei, K. Wang, X. Li, Mössbauer study of cobalt ferrite nanocrystals substituted with rare-earth Y^{3+} ions, *J. Magn. Magn. Mater.*, 321 (2009) 1155–1158.
- [3] J. Judith Vijaya, G. Sekaran, M. Bououdina, Effect of Cu^{2+} doping on structural, morphological, optical and magnetic properties of $MnFe_2O_4$ particles/sheets/flakes-like nanostructures, *Ceram. Int.*, 41 (2015) 15–26.
- [4] J. Popplewell, L. Sakhnini, The dependence of the physical and magnetic properties of magnetic fluids on particle size, *J. Magn. Magn. Mater.*, 149 (1995) 72–78.
- [5] K. Manjunatha, I.C. Sathish, S.P. Kubrin, A.T. Kozakov, T.A. Lastovina, A. V. Nikolskii, K.M. Srinivasamurthy, Mehaboob Pasha, V. Jagadeesha Angadi, X-ray photoelectron spectroscopy and low temperature Mössbauer study of Ce^{3+} substituted $MnFe_2O_4$ *J. Mater. Sci. Mater. Electron.*, 30 (2019) 10162–10171.
- [6] K. Raj, B. Moskowitz, R. Casciari, Advances in ferrofluid technology, *J. Magn. Magn. Mater.*, 149 (1995) 174–180.
- [7] V.G. Harris, A. Geiler, Y. Chen, S.D. Yoon, M. Wu, A. Yang, Z. Chen, P. He, P. V. Parimi, X. Zuo, Recent advances in processing and applications of microwave ferrites, *J. Magn. Magn. Mater.*, 321 (2009) 2035–2047.
- [8] S.E. Jacobo, J.C. Apesteguy, N.N. Shegoleva, G. V Kurlyandskaya, Structural and magnetic properties of nanoparticles of NiCuZn ferrite prepared by the selfcombustion method, in: *Solid State Phenom.*, Trans Tech Publ., 168 (2011) 333–340.
- [9] R. Steiner, K. Merle, H.G. Andresen, A high-precision Ferrite-induction beam-current monitoring system, *Nucl. Instruments Methods*. 127 (1975) 11–15.
- [10] A. Sutka, G. Mezinskis, A. Lasis, M. Stingaciu, Gas sensing properties of Zn-doped ptype nickel ferrite, *Sensors Actuators B Chem.*, 171 (2012) 354–360.
- [11] X. Wu, Z. Ding, N. Song, L. Li, W. Wang, Effect of the rare-earth substitution on the structural, magnetic and adsorption properties in cobalt ferrite nanoparticles, *Ceram. Int.*, 42 (2016) 4246–4255.
- [12] A. Verma, M.I. Alam, R. Chatterjee, T.C. Goel, R.G. Mendiratta, Development of a new soft ferrite core for power applications, *J. Magn. Magn. Mater.*, 300 (2006) 500–505.
- [13] V. Jagadeesha Angadi, K. Manjunatha, K. Praveena, Vinayak K. Pattar, Brian Jeevan Fernandes, S.O. Manjunatha, Jakeer Husain, S.V. Angadi, L.D. Horakeri, K.P. Ramesh, Magnetic properties of larger ionic radii samarium and gadolinium doped manganese zinc ferrite nanoparticles prepared by solution combustion method, *J. Magn. Magn. Mater.*, 529 (2021) 167899.
- [14] Salma Ikram, Jolly Jacob, K. Mahmood, A. Ali, N. Amin, U. Rehman, M. Imran Arshad, M. Ajaz un Nabi, Kashif Javid, A. Ashfaq, M. Sharif, S. Hussain, Influence of Ce^{3+} substitution on the structural, electrical and magnetic properties of $Zn_{0.5}Mn_{0.43}Cd_{0.07}Fe_2O_4$ spinel ferrites, *Physica B Condens. Matter*, 580 (2020) 411764.
- [15] B.P. Rao, B. Dhanalakshmi, S. Ramesh, P.S.V.S. Rao, Cation distribution of Ni-Zn-Mn ferrite nanoparticles, *J. Magn. Magn. Mater.*, 456 (2018) 444–450.

- [16] R.C. Bharamagoudar, Jagadeesha Angadi, A.S. Patil, L.B. Kankanawadi, S. N. Mathad. Structural and Dielectric Properties of Combustion-Synthesized Mn-Zn Nanoferrites. *Int. J Self-Propag. High-Temp. Synth.* 28, 132–136 (2019).
- [17] K. Qian, Z. Yao, H. Lin, J. Zhou, A. A. Haidry, T. Qi, W. Chen, X. Guo, The influence of Nd substitution in Ni–Zn ferrites for the improved microwave absorption properties, *Ceram. Int.*, 46 (2020) 227–235.
- [18] Asim Anwar, Sonia Zulfiqar, Muhammad Asif Yousuf, Sameh A. Ragab, Muhammad Azhar Khand, Imran Shakir, Muhammad Farooq Warsi, Impact of rare earth Dy⁺³ cations on the various parameters of nanocrystalline nickel spinel ferrite, *J. Mater. Res. Technol.*, 9 (2020) 5313–5325.
- [19] K. Manjunatha, V. Jagadeesha Angadi, R. Rajaramakrishna, U. Mahaboob Pasha, Role of 5 mol% Mg–Ni on the Structural and Magnetic Properties of Cobalt Chromates Crystallites Prepared by Solution Combustion Technique, *J. Supercond. Nov. Magn.*, 33 (2020) 2861–2866.
- [20] K. Manjunatha, K.M. Srinivasamurthy C.S. Naveen, Y.T. Ravikiran, E.I. Sitalo, S.P. Kubrin, Siddaling Matteppanavar, N. Sivasankara Reddy, V. Jagadeesha Angadi, Observation of enhanced humidity sensing performance and structure, dielectric, optical and DC conductivity studies of scandium doped cobalt chromate, *J. Mater. Sci: Mater. Electron.* 30 (2019) 17202–17217.
- [21] K. Manjunatha, V. Jagadeesha Angadi, R.A.P. Ribeiro, M.C. Oliveira, S. R. de Lázaro, M.R.D. Bomio, S. Matteppanavar, S. Rayaprol, P. D. Babu, U. Mahaboob Pasha, Structural, Electronic and Magnetic properties of Sc³⁺ doped CoCr₂O₄ nanoparticles, *New J. Chem.*, 44 (2020) 14246–14255.
- [22] I.C. Sathisha, K. Manjunatha, V. Jagadeesha Angadi, Ranjeth Kumar Reddy, Structural, Microstructural, Electrical, and Magnetic Properties of CuFe_{2-(x+y)}Eu_xSc_yO₄ (where x and y vary from 0 to 0.03) Nanoparticles, *J. Supercond. Nov. Magn.*, 33 (2020) 3963–3973.
- [23] H.R. Lakshmiprasanna, K. Manjunatha, V. Jagadeesha Angadi, U. Mahaboob Pasha, Jakeer Husain, Effect of cerium on structural, microstructural, magnetic and humidity sensing properties of Mn–Bi ferrites, *Nano-Struct. Nano-Objects*, 24 (2020) 100608.
- [24] I.C. Sathisha, K. Manjunatha, Anna Bajorek, B. Rajesh Babu, B. Chethan, T. Ranjeth Kumar Reddy, Y.T. Ravikiran, V. Jagadeesha Angadi, Enhanced Humidity Sensing and Magnetic Properties of Bismuth doped Copper ferrites for Humidity sensor Applications, *J. Alloy Compd.*, 848 (2020) 156577 .
- [25] M. Abhishek, K. Manjunatha, V. Jagadeesha Angadi, E. Melagiriappa, B. N. Anandaram, H.S. Jayanna, M. Veena, K. Swaroop Acharya, Structural and magnetic properties of Eu³⁺ substituted Mg–Cd nanoferrites: A detailed study of Influence of high energy γ -rays irradiation, *Chem. Data Coll.*, 28 (2020) 100460.
- [26] K.M. Srinivasamurthy, K. Manjunatha, E.I. Sitalo, S.P. Kubrin, I.C. Sathish, S. Matteppanavar, B. Rudraswamy, V.J. Angadi, Effect of Ce³⁺ substitution on the structural, morphological, dielectric, and impedance spectroscopic studies of Co–Ni ferrites for automotive applications, *Indian J. Phys.*, 94 (2020) 593–604.
- [27] E. Melagiriappa, H.S. Jayanna, B.K. Chougule, Dielectric behavior and ac electrical conductivity study of Sm³⁺ substituted Mg–Zn ferrites, *Mater. Chem. Phys.*, 2008, 112, 68–73.

- [28] R.C. Kambale, P.A. Shaikh, C.H. Bhosale, K.Y. Rajpure, Y.D. Kolekar, Dielectric properties and complex impedance spectroscopy studies of mixed Ni-Co ferrites, *Smart Mater. Struct.*, 18 (2009) 085014.
- [29] K. Manjunatha, V. Jagadeesha Angadi, M.C. Oliveira, S.R. de Lazaro, E. Longo, R.A.P. Ribeiro, S.O. Manjunatha, N.H. Ayachit, Towards shape-oriented Bi-doped CoCr_2O_4 nanoparticles from theoretical and experimental perspective: Structural, Morphological, Optical, Electrical and Magnetic properties, *J. Mater. Chem. C*, 9 (2021) 6452-6469.
- [30] Somsack Vangchangyia, Ekaphan Swatsitang, Prasit Thongbai, Supree Pinitsoontorn, Teerapon Yamwong, Santi Maensiri, Vittaya Amornkitbamrung, Prinya Chindaprasirt, Very Low Loss Tangent and High Dielectric Permittivity in Pure- $\text{CaCu}_3\text{Ti}_4\text{O}_{12}$ Ceramics Prepared by a Modified Sol-Gel Process, *J. Am. Ceram. Soc.*, 95 (2012) 1497-1500.
- [31] K. Manjunatha, V. Jagadeesha Angadi, K. M. Srinivasamurthy, Shidaling Matteppanavar, Vinayak K. Pattar and U. Mahaboob Pasha, Exploring the Structural, Dielectric and Magnetic Properties of 5 Mol% Bi^{3+} -Substituted CoCr_2O_4 Nanoparticles, *J. Supercond. Nov. Magn.*, 33 (2020) 1747-1757.
- [32] S.I.R. Costa, M. Li, J.R. Frade, D.C. Sinclair, Modulus spectroscopy of $\text{CaCu}_3\text{Ti}_4\text{O}_{12}$ ceramics: clues to the internal barrier layer capacitance mechanism, *RSC Adv.*, 3 (2013) 7030-7036.
- [33] K. Iwauichi, *J. Appl. Phys.*, Dielectric properties of fine particles of Fe_3O_4 and some ferrites, 10 (1971) 1520-1528.
- [34] V. Jagadeesha Angadi, H.R. Lakshmiprasanna, K. Manjunatha, Investigation of Structural, Microstructural, Dielectrical and Magnetic Properties of Bi^{3+} Doped Manganese Spinel Ferrite Nanoparticles for Photonic Applications, *Bismuth - Fundamentals and Photonic Applications*, IntechOpen (2020), ISBN: 978-1-83968-243-8. DOI: 10.5772/intechopen.92430.
- [35] K.P. Padmasree, D.D. Kanchan, A.R. Kulkarni, Impedance and modulus studies of the solid electrolyte system $20\text{Cd}_{12-80}[\text{xAg}_{20-y} (0.7 \text{V}_2\text{O}_5-0.3 \text{B}_2\text{O}_3)]$, where $1 \leq x/y \leq 3$, *Solid State Ion.* 177 (2006) 475.
- [36] U. Ghazanfar, S.A. Siddiqi, G. Abbas, Study of room temperature dc resistivity in comparison with activation energy and drift mobility of NiZn ferrites, *Mater. Sci. Eng. B* 118 (2005) 132.
- [37] T. Badapanda, S. Sarangi, S. Parida, B. Behera, B. Ojha and S. Anwar, Frequency and temperature dependence dielectric study of strontium modified Barium Zirconium Titanate ceramics obtained by mechanochemical synthesis, *J. Mater. Sci. Mater. Electron.*, 26 (2015) 3069.
- [38] K. Kamala Bharathi, J. Arout Chelvane and G. Markandeyulu, Magnetoelectric properties of Gd and Nd-doped nickel ferrite, *J. Magn. Magn. Mater.*, 321 (2009) 3677-3680.
- [39] K. Manjunatha, V. Jagadeesha Angadi, K.M. Srinivasamurthy, Shidaling Matteppanavar, Synthesis and Study of Structural, Dielectric Properties of $\text{Co}_{0.95}\text{Bi}_{0.05}\text{Cr}_2\text{O}_4$ nanoparticles, *AIP Conf. Proc.*, 2274, 020004 (2020).
- [40] Hafiz Muhammad, Tahir Farid, Ishtiaq Ahmad, Irshad Ali, Shahid M. Ramay, Asif Mahmood, G. Murtaza, Dielectric and impedance study of praseodymium substituted Mg-based spinel ferrites, *J. Magn. Magn. Mater.*, 434 (2017) 143-150.